HHS Public Access

Author manuscript

J Bone Miner Res. Author manuscript; available in PMC 2022 October 03.

Published in final edited form as:

J Bone Miner Res. 2013 September ; 28(9): 1962–1974. doi:10.1002/jbmr.1935.

Targeted Disruption of Leucine-Rich Repeat Kinase 1 But Not Leucine-Rich Repeat Kinase 2 in Mice Causes Severe Osteopetrosis

Weirong Xing[1,2], **Jeff Liu**[3], **Shaohong Cheng**[1], **Peter Vogel**[4], **Subburaman Mohan**[1,2,*], **Robert Brommage**[3,*]

[1]Musculoskeletal Disease Center, Jerry L. Pettis Memorial VA Medical Center, Loma Linda, CA, USA

[2]Department of Medicine, Loma Linda University, Loma Linda, CA, USA

[3]Department of Metabolism, Lexicon Pharmaceuticals, The Woodlands, TX, USA

[4]Department of Pathology, Lexicon Pharmaceuticals, The Woodlands, TX, USA

Abstract

To assess the roles of *Lrrk1* and *Lrrk2,* we examined skeletal phenotypes in *Lrrk1* and *Lrrk2* knockout (KO) mice. *Lrrk1* KO mice exhibit severe osteopetrosis caused by dysfunction of multinucleated osteoclasts, reduced bone resorption in endocortical and trabecular regions, and increased bone mineralization. *Lrrk1* KO mice have lifelong accumulation of bone and respond normally to the anabolic actions of teriparatide treatment, but are resistant to ovariectomy-induced bone boss. Precursors derived from *Lrrk1* KO mice differentiate into multinucleated cells in response to macrophage colony-stimulating factor (M-CSF)/receptor activator of NF-κB ligand (RANKL) treatment, but these cells fail to form peripheral sealing zones and ruffled borders, and fail to resorb bone. The phosphorylation of cellular Rous sarcoma oncogene (c-Src) at Tyr-527 is significantly elevated whereas at Tyr-416 is decreased in *Lrrk1*-deficient osteoclasts. The defective osteoclast function is partially rescued by overexpression of the constitutively active form of Y527F c-Src. Immunoprecipitation assays in osteoclasts detected a physical interaction of Lrrk1 with C-terminal Src kinase (Csk). *Lrrk2* KO mice do not show obvious bone phenotypes. Precursors derived from *Lrrk2* KO mice differentiate into functional multinucleated osteoclasts. Our finding of osteopetrosis in *Lrrk1* KO mice provides convincing evidence that Lrrk1 plays a

Address correspondence to: Subburaman Mohan, PhD, Musculoskeletal Disease Center, Jerry L Pettis VA Medical Center, 11201 Benton Street, Loma Linda, CA 92357, USA. Subburaman.Mohan@va.gov.

The present address of Peter Vogel is Department of Pathology, St. Jude Children's Research Hospital, Memphis, TN 38105, USA.

*SM and RB are co-senior authors.

Authors' roles: Study design: WX, SM, and RB. Acquisition of data: WX, JL, SC, and RB. Analysis and interpretation of data: WX, JL, PV, SM, and RB. Drafting manuscript: WX, SM, and RB. Revising manuscript: WX, SM, and RB. Approved final version of manuscript: WX, JL, SC, PV, SM, and RB. SM accepts responsibility for integrity of data analysis.

Disclosures

JL, PV, and RB were employees of Lexicon Pharmaceuticals when the studies were performed, and JL and RB own stock and stock options. Lexicon Pharmaceuticals partially supported the studies presented in this work. All other authors state that they have no conflict of interest.

Additional Supporting Information may be found in the online version of this article.

critical role in negative regulation of bone mass in part through modulating the c-Src signaling pathway in mice.

Keywords

OSTEOCLAST; BONE RESORPTION; BONE DENSITY; KNOCKOUT; PIT FORMATION; CSK; c-SRC

Introduction

Bone remodeling is an essential process that regulates skeletal integrity, bone mineral density (BMD), and bone strength throughout life. The maintenance of BMD is controlled by the activities of two specialized cells within bone that have antagonistic activities but modulate two coupled processes.[1] Osteoblasts synthesize and deposit bone matrix and increase bone mass, whereas osteoclasts degrade mature and newly synthesized bone upon activation.[1-3] Disturbances of bone homeostasis cause either osteopetrosis or osteoporosis, conditions in which bone mass is increased or decreased, respectively. Osteoporosis is a common disease that is characterized by an age-dependent decrease in BMD and microarchitectural deterioration of bone with increased risk of fragility fractures of the hip, spine, and other skeletal sites.[4] Two major causes of osteoporosis are low peak BMD, typically achieved around the age of 30 years, and high bone loss rate after menopause and during aging. This bone loss occurs because bone resorption exceeds bone formation. The pathogenesis of several localized bone diseases, such as rheumatoid arthritis, periodontal disease, and multiple myeloma, also involve increased bone resorption.[5-7] Inhibitors of bone resorption such as bisphosphonates and receptor activator of NF-κB ligand (RANKL) antibody are employed to treat bone diseases. These inhibitors act via inhibiting both osteoclast formation and osteoclast activity. Long-term treatment with these drugs may be associated with impaired fracture healing as well as osteonecrosis of the jaw.[8-11] It is, therefore, important to develop new drug targets that are specific and exhibit little or no side effects during long-term therapy.

Leucine rich repeat kinase 1 (LRRK1) belongs to the ROCO protein family,[12-14] and contains four ankyrin repeats, seven leucine-rich repeats, a guanosine triphosphatase (GTPase)-like domain of Ras of complex proteins (Roc), a C-terminal of Roc (COR) domain, and a serine/threonine kinase domain.[15] LRRK2,a homolog, contains most domains of the ROCO family protein and an extra LRRK2-specific repeat at the N-terminus, but lacks ankyrin repeats. Both LRRK1 and LRRK2 are functional protein kinases and guanosine diphosphatase (GDP)/guanosine triphosphate (GTP)-binding proteins, and are ubiquitously expressed in multiple tissues.[16,17] Binding of GTP to LRRK1 is specific, requires the GTPase-like Roc domain, and leads to kinase autoactivation.[18] There are at least three candidate tyrosine phosphorylation sites for additional regulation[19,20] Phosphorylation of Tyr-94 in the ankyrin repeat might regulate protein binding whereas phosphorylation of Tyr-1453 in the kinase domain of human LRRK1 regulates kinase activity.[19] More recent studies have found that phosphorylation of Tyr-944 in the ROC domain is stimulated by epidermal growth factor (EGF) treatment.[20] In terms of functions

of LRRK2, several linkage studies have demonstrated that mutations in the *Lrrk2* gene in humans are linked to Parkinson's disease.[15,21,22] Mice lacking Lrrk2 protein showed an early-onset increase in number and size of secondary lysosomes in kidney cells and lamellar bodies in lung cells whereas mice having an Lrrk2 kinase-dead mutant protein from the endogenous locus displayed similar early-onset pathophysiological changes in the kidneys but not the lungs.[23] However, the functions of LRRK2 in bone, the association of LRRK1 mutations with human diseases, and LRRK1/2 signaling pathways are unknown.

To directly investigate the roles of these two kinases in vivo, we characterized the bone phenotypes of *Lrrk1* and *Lrrk2* knockout (KO) mice. Although both proteins are present in osteoclasts,[17] lack of Lrrk1 but not Lrrk2 induces severe osteopetrosis resulting from dysfunctional osteoclasts. Furthermore, our findings demonstrate for the first time that the Lrrk1 effect on osteoclast activity is mediated in part via regulation of C-terminal Src kinase/cellular Rous sarcoma oncogene (Csk/c-Src) signaling.

Materials and Methods

Recombinant proteins, antibodies, and plasmids

Recombinant macrophage colony-stimulating factor (M-CSF) and RANKL proteins were from R&D Systems (Minneapolis, MN, USA). Anti-c-Src and anti-Csk antibodies were products of Cell Signaling Technology (Danvers, MA, USA). A monoclonal antibody against Flag (M5) was purchased from Sigma (St. Louis, MO, USA). Alexa Fluor 488 phalloidin was obtained from Invitrogen (Carlsbad, CA, USA). Plasmid pMX-IRES-EGFP was kindly provided by Dr. Matsuo of the Keio University, Japan. The pcDNA-hLrrk1-Flag plasmid was a gift from Dr. Daechsel of the Mayo Clinic, Jacksonville, FL, USA. Constructs of pLNCX chick Src Y527F (Addgene #13660) were provided by Dr. Joan Brugge of Harvard Medical School, Boston, MA, USA.

Mice

Lrrk1-deficient ($Lrrk1^{-/-}$) mice were generated via targeted disruption of coding exons 16 through 19 (exons numbered according to accession NM_146191.3) of the GTPase domain of the *Lrrk1* gene by homologous recombination as described in Supplemental Fig. 1. *Lrrk2* KO mice with targeted deletion of exons 39 and 40 were purchased from The Jackson Laboratory (Bar Harbor, ME, USA). Mice were housed at the Jerry L. Pettis Memorial VA Medical Center Veterinary Medical Unit (Loma Linda, CA, USA) or at the Lexicon Pharmaceuticals animal facility (The Woodlands, TX, USA) under standard approved laboratory conditions. All procedures were performed with approval of the Institutional Animal Care and Use Committees of the two institutions.

High-throughput screening of BMD

A total of 3629 distinct gene KO lines (45,893 mice) were evaluated by high-throughput dual-energy X-ray absorptiometry (DXA) scans. Gene KO involved both gene trap (1329 distinct gene KO lines) and homologous recombination (2300 distinct gene KO lines) technologies as described.[24,25] Mice underwent body (excluding the head) scans using a PIXImus DXA (GE/Lunar, Madison, WI, USA) scanner at 14 weeks of age as described.[26]

From body BMD, volumetric vBMD was calculated by dividing BMD by the square root of measured bone area. For each line, mean KO vBMD/mean wild-type (WT) littermate vBMD was calculated for both male and female mice, and these male and female values were averaged, yielding a normalized vBMD value. When there were uneven distributions of male and female mice, values for normalized vBMD were weighted for the actual number of mice analyzed. Spine and femur BMD were also acquired for each KO line.[26]

Evaluation of bone architectures

Microarchitecture of the femurs, tibia, and spine from 8-week-old mice was assessed by micro–computed tomography (μCT) at Loma Linda (Scanco vivaCT 40; Scanco Medical, Brüttisellen, Switzerland) as described.[27-29] All additional μCT scans were performed at Lexicon (Scanco μCT40) as reported.[30] For cortical bone, 20 slices were analyzed at the femoral proximal shaft, tibia midshaft, and tibia-fibular junction sites. For femoral neck, 20 slices exhibiting the lowest total area were analyzed. For lumbar vertebra 5 (L_5), 150 slices in the mid-region were analyzed that excluded primary spongiosa.

Bone histomorphometry

Eight-week-old mice were injected intraperitoneally with calcein (20 mg/kg) 8 days and 2 days prior to euthanization by CO_2 to label mineralizing bone surfaces. Mouse femurs were fixed in 10% formalin overnight, washed, dehydrated, and embedded in methyl methacrylate resin for sectioning. The sampling sites and histomorphometric methods used have been described.[29] Trabecular surface and tartrate-resistant acid phosphatase (TRAP)-labeled trabecular surface were measured in a blinded fashion with computer software OsteoMeasure (OsteoMetrics, Decatur, GA, USA).[31,32] The mineral apposition rate (MAR) and bone formation rate (BFR)/bone surface (BS) were calculated as described.[33]

Ovariectomy surgery

Female mice were anesthetized with isoflurane (3% to 4%) for bilateral ovariectomy (OVX) or sham surgery at 16 weeks of age. The ovaries were removed from the mice by dorsal incision into the region between the dorsal hump and the base of the tail. A ligature was placed, and both ovaries were removed. DXA scans were performed at baseline and weeks 4, 8, and 12 postsurgery.

Parathyroid hormone treatment

Male mice at 70 weeks of age were given daily subcutaneous injections of teriparatide (80 μg/kg) for 8 consecutive days. Blood was collected at baseline and again 24 hours after the last dose for serum N-terminal propeptide of collagen type I (P1NP) measurements.

Serum measurements

Serum levels of P1NP, collagen type 1 C-terminal telopeptide (Ctx-1), and TRAP5b were determined using rat/mouse P1NP, RatLaps, and mouse TRAP5b EIA kits, respectively, from Immunodiagnostic Systems (Fountain Hills, AZ, USA), according to the manufacturer's instructions and a previous report.[34] Serum alkaline phosphatase (ALP) activity was measured in samples diluted 1:40 as reported.[35]

RNA extraction and RT-PCR

RNA was extracted from primary cultures as described.[28] An aliquot of RNA (2 μg) was reverse-transcribed into cDNA in a 20-μL reaction volume with an oligo$(dT)_{12\text{-}18}$ primer. An aliquot of 0.5 μL template cDNA was used for PCR in the presence of 100 nM of specific forward and reverse primers in a 50-μL reaction volume. Primers specific to β-actin were used as internal controls. PCR products were separated by electrophoresis in 1% agarose gels.

Murine leukemia virus–based viral transduction

Murine leukemia virus (MLV)-based viral particles were generated in Plat-E cells, and transduction of primary osteoclast precursors was carried out with a ViraDuctin retrovirus transduction kit, according to the manufacturer's instructions (Cell Biolabs, San Diego, CA, USA).

In vitro osteoclast formation

Primary osteoclast precursors were isolated from the spleen or bone marrow of femur and tibia from 5-week-old mice as described.[36] The isolated precursors were maintained in α modified essential medium (α-MEM supplemented with 10% fetal bovine serum (FBS), penicillin (100 units/mL), streptomycin (100 μg/mL), and macrophage colony stimulating factor (M-CSF) (20 ng/mL) at 37°C in 5% CO_2 for 3 days to stimulate monocyte proliferation. To induce osteoclast differentiation, trypsinized precursors were seeded in 48-well plates (5000 cells/well), and incubated with M-CSF (20 ng/mL) and RANKL (30 ng/mL). The medium was changed every 2 days. Osteoclastogenesis was evaluated by counting TRAP-positive multinucleated cells having at least three nuclei.

Bone resorption pit and actin ring formation assays

Slices from bovine cortical bone were placed in 48-well plates and cells were differentiated on top of the bone slices as described in the previous section. Cells on bone slices were digested with trypsin at 37°C overnight. Multinucleated cells were further removed by 5-minute sonication in 1 M ammonia. Air-dried bone slices were stained with hematoxylin. The entire surface of each bone slice was examined and the total resorbed area per bone slice was quantified using ImageJ software (National Institutes of Health). Resorption pits were also visualized by nano-CT at a voxel dimension of 0.3 μm (VersaXRM-500; Xradia, Pleasanton, CA, USA). Cells on bone slices were also stained with Alexa Fluor488 conjugated phalloidin for F-actin, and 4,6-diamidino-2-phenylindole (DAPI) for nuclei location. Actin ring formation, sealing zone, and 3D osteoclast images were visualized by confocal microscopy.

Immunoprecipitation

RAW264.7 cells were transfected with pcDNA-Flag/hLrrk1 or pcDNA-GFP by nucleofection (Lonza Group, Basel, Switzerland). Cells were cultured in α-MEM containing 10% FBS, 30 ng/mL of RANKL, and 20 ng/mL of M-CSF for 4 days, lysed with lysis buffer, and precleared with protein A/G Sepharose prior to immunoprecipitation with anti-

Flag or control immunoglobulin G (IgG). Interactions of Lrrk1 with Csk were detected by Western blot using anti-Csk.[29]

Western blot analyses

Cultured osteoclasts were lysed as described in the previous section. Cell lysate (30 μg cellular protein) was separated by 8% SDS-PAGE under reducing conditions for Western blot analyses with specific antibodies against c-Src, Csk, Flag, and β-actin as described.[37]

Statistical analyses

Data are expressed as mean ± SEM and were analyzed using Student's *t* test or two-way ANOVA (Fig. 6 C). Values were considered statistically significant when $p < 0.05$.

Results

Lrrk1-deficient mice exhibit profound osteopetrosis

Lrrk1$^{-/-}$ mice were born alive, with the expected Mendelian frequency at 2 weeks of age. The body length of the *Lrrk1* KO mice was slightly shorter compared to the WT control littermates at 4 weeks of age (data not shown). Targeted disruption of *Lrrk1* resulted in the highest observed body vBMD of the 3629 distinct gene KO lines examined, with a *Z*-score of 9.0 above the mean by DXA high-throughput screening (Fig. 1A). The vBMD of *Lrrk1* KO mice was higher than *Sost* and *c-Src* KO mice. Total body BMD measured by DXA was increased by 40% in both *Lrrk1* KO males and females at 6 weeks of age (Fig. 1B). In contrast, heterozygous mice having a single copy of *Lrrk1* did not exhibit a significant difference in total body BMD compared to control mice (data not shown). Both *Lrrk1* KO males and females have the same elevation in total BMD as compared to WT gender-matched littermate mice. At 70 weeks of age, DXA BMD in male KO mice was elevated by 65% for total body, 85% for femur, and 190% for spine (Fig. 1C).

μCT analyses of trabecular bone of the vertebral body from 8-week-old females revealed that the trabecular bone volume to total volume was increased 2.3-fold in *Lrrk1* KO mice compared to littermate controls (Fig. 2A, upper panel). Trabecular number and trabecular thickness were elevated 50% and 100%, respectively, while trabecular separation was decreased 43% in the KO mice (Fig. 2B-D). The trabecular bone of *Lrrk1* KO tibias was also increased (Fig. 2E). Consistent with DXA data in aging mice, trabecular bone volume to total volume in a 1.2-mm-thick region of L_5 mid-vertebral body was increased 5.2-fold in *Lrrk1* KO mice at 79 weeks of age compared to the control littermates (Fig. 2A, lower panel). As expected, trabecular bone density was reduced in WT aging 79-week-old mice compared to the young 8-week-old mice (Fig. 2A). However, age-related bone loss did not occur in *Lrrk1* KO mice as trabecular BMD measurements remained relatively stable across various age groups. The lengths of the femur and tibia in *Lrrk1* KO mice were reduced by 9% and 11% ($p < 0.01$, data not shown). Long bones have a wider metaphysis, normal diaphysis, but reduced marrow cavity area (Fig. 2G). To avoid biases in determining the trabecular/cortical interface in μCT scans, midshaft tibia, tibia-fibular junction, and proximal femur shaft were selected for having no trabecular bone in the marrow cavity. Cortical thickness at the tibia-fibular junction region was increased by 7% in 8-week-old *Lrrk1* KO

mice as compared to littermate controls (Fig. 2F). Disruption of *Lrrk1* also resulted in increased cortical bone thickness in the midshaft tibia, tibia-fibular junction, and proximal femur shaft in 79-week-old male mice (Fig. 2G, H). Increased cortical thickness resulted from reduced endocortical resorption, as total area (diameter) was unaffected and marrow cavity area was reduced by 20% ($p = 0.002$) in the midshaft tibia, 28% ($p < 0.001$) at the tibia-fibular junction, and 10% ($p = 0.08$) in the proximal femur shaft. There is evidence of cortical bone hypermineralization as indicated by material BMD values, which were elevated by 3.3% in the midshaft tibia, 2.9% at the tibia-fibular junction, and 4.4% in the proximal femur shaft ($p < 0.02$ at all sites). Examination of undecalcified femur cortical bone sections revealed no obvious differences in osteocyte density (data not shown).

Histological analyses confirmed a severe osteopetrotic phenotype in *Lrrk1* KO mice. Decalcified bone sections showed that there was extensive unresorbed cartilage below the growth plate of the distal femur and proximal tibia of *Lrrk1* KO mice, and numerous TRAP-positive osteoclasts with increased trabecular number and trabecular bone volume (Fig. 3A, B). The primary spongiosa in the *Lrrk1* KO mice extended to the diaphysis and was characterized by increased mature osteoclasts, cartilage, and trabecular bone. The secondary spongiosa were very short and incomplete (Fig. 3B). The trabecular bone volume to total volume was increased by 2.2-fold but osteoclast surface to bone surface was not changed in *Lrrk1* KO mice at the secondary spongiosa (Fig. 3C, D). Similarly, markedly increased trabecular number and thickness were also evident in the vertebrae from 79-week-old *Lrrk1* KO mice (Fig. 4A). Interestingly, all osteopetrotic areas appeared to contain increased numbers of abnormal osteoclasts. The *Lrrk1* KO osteoclast contained increased amounts of pale eosinophilic cytoplasm with enlarged unclumped nuclei. The elongation of the primary spongiosa with retention of cartilage cores indicates the osteoclasts have markedly impaired resorptive activity. The mineral apposition rate (MAR) and bone formation rate/bone surface (BFR/BS) were significantly reduced by 44% and 50%, respectively, in *Lrrk1* KO mice (Fig. 4B-D).

Histological examinations of teeth and surrounding bones at 79 weeks of age found that *Lrrk1* KO mice had normal incisors, molars, and periodontal ligaments. The turbinate bones were of normal thickness and contained prominent basophilic (reversal) lines. There was modest osteosclerosis of the periodontal bone, nasal septum, and bridge of the nose. No soft tissue abnormalities were noted (data not shown).

Analyses of serum chemistry values from *Lrrk1* KO and WT control littermates showed that TRAP5b, a marker of osteoclast number, was elevated by 63% in young mice and 112% in older mice (Fig. 5A). Serum ALP activity was reduced by 15% in *Lrrk1* KO mice at 8-week-old (Fig. 5B). Serum Ctx-1 level, a marker for osteoclast activity, was decreased by 67% in *Lrrk1* KO male mice at 4 weeks of age compared to the corresponding WT control mice (Fig. 5C).

Lrrk1 KO mice have a normal anabolic response and are resistant to OVX-induced bone loss

Consistent with osteopetrosis, male KO mice at 70 weeks of age had a 45% reduction in serum levels of P1NP (Fig. 5D). Treating mice with teriparatide at 80 μg/kg daily for 8 days,

increased serum P1NP values 4.1-fold in WT mice and 6.0-fold in *Lrrk1* KO mice. At the end of teriparatide treatment, serum P1NP levels were identical in teriparatide-treated WT and teriparatide-treated *Lrrk1* KO mice.

To evaluate the possible protection of bone loss following OVX by disruption of the *Lrrk1* gene, mice underwent sham or bilateral OVX at 16 weeks of age. Skeletal changes were followed by longitudinal DXA scans at 4, 8, and 12 weeks postsurgery and μCT analyses after necropsy at 12 weeks. As described earlier, *Lrrk1* KO mice had elevated total body BMD (40%), spine BMD (64%), and femur BMD (65%) at the time of OVX. As shown in Fig. 6, OVX produced bone loss in WT but not *Lrrk1* KO mice. Reductions in spine, total body, and femur BMD after 12 weeks of OVX were statistically significant in WT mice but there were no statistically significant BMD changes with OVX in *Lrrk1* KO mice (Fig. 6A-D). These DXA observations were confirmed by μCT analyses. *Lrrk1* KO mice had increased bone mass in the femoral neck, midtrabecular region of L_5, and mid-shaft tibia, and these mice were resistant to OVX-induced bone loss at all three skeletal sites. In contrast, WT mice lost bone at all three skeletal sites following OVX (Fig. 6E-G).

Osteoclasts lacking Lrrk1 have defective bone resorptive activity

Findings of plentiful osteoclasts in histological sections and elevated serum TRAP5b levels in *Lrrk1* KO mice, along with normal osteoclast differentiation and bone nodule formation in cultures derived from *Lrrk1*-deficient bone marrow (Supplemental Fig. 2), all suggest that Lrrk1 is essential for osteoclast function. To evaluate this possibility, resorption pit formation assays were performed using osteoclasts generated from *Lrrk1* KO and WT mice. Although the number of mature TRAP-positive osteoclasts on bone slices were comparable for osteoclast preparations generated from KO and WT mice (Fig. 7A), the lack of *Lrrk1* in osteoclasts significantly impaired their ability to resorb bone. The area of resorption pits was reduced by 85% in *Lrrk1* KO cells compared to WT cells (Fig. 7B, D). In addition, individual resorption pits appeared smaller and shallower in KO cultures as measured by nano-CT (Fig. 7C).

Lrrk1-deficient osteoclasts fail to form a peripheral sealing zone and ruffled border on bone slices

As shown in Fig. 8, more than 90% of WT mature osteoclasts displayed a typical rounded appearance with clear actin ring formation (Fig. 8A, C). Horizontal cross-section images of multinucleated cells revealed clustered F-actin formed a peripheral sealing zone in WT osteoclasts from both views when cultured on bone slices (arrows in Fig. 8B, left panel). In contrast, most *Lrrk1* KO multinucleated cells showed diffuse F-actin in the cytoplasm with weak peripheral F-actin rings. Despite contact with the bone surface, fewer than 5% of the *Lrrk1* KO osteoclasts formed a typical sealing zone (Fig. 8B, right panel), and these cells are extremely large, round, and flat on bone slices.

Lrrk1 interacts with Csk and is involved in regulation of c-Src phosphorylation

Because the phenotypic characteristics of *Lrrk1* KO cells in vitro, and osteopetrotic phenotype of *Lrrk1* KO mice are similar to c-Src–deficient cells and c-Src KO mice, [38-40] we examined the status of c-Src phosphorylation in WT and *Lrrk1* KO osteoclasts.

Phosphorylation of c-Src at Tyr-527 was significantly elevated by 130% in *Lrrk1*-deficient osteoclasts, whereas total c-Src protein levels were unchanged (Fig. 9A, B). By contrast, phosphorylation of c-Src at Tyr-416 was significantly reduced by 70% in *Lrrk1* KO cells. Since Csk phosphorylates c-Src,[41] we determined if Lrrk1 interacts with Csk. Figure 9C, D shows that Lrrk1 immunoprecipitated with Csk in RAW264.7 cells overexpressing flag-tagged hLrrk1.

Rescue of *Lrrk1*$^{-/-}$ osteoclast function by overexpression of Y527F *Src*

To determine whether dysfunction of *Lrrk1*-deficient osteoclasts results from reduced c-Src signaling, we performed a rescue experiment by overexpressing constitutively active Y527F c-Src in primary osteoclast precursors, and examining mature osteoclasts' bone resorptive activity after RANKL and M-CSF treatment. As shown in Fig. 9E, approximately 80% of osteoclasts derived from *Lrrk1* KO mice were transduced by MLV virus, and expressed a high level of GFP marker protein. MLV-mediated overexpression of constitutively active c-Src partially rescued *Lrrk1*$^{-/-}$ osteoclast function, as measured using F-actin ring formation and pit formation assays (Fig. 9F, G). WT osteoclasts contained single or multiple clear actin rings, and the cells appeared to have migrated on the bone slice. In contrast, most of control *Lrrk1*-deficient osteoclasts expressing GFP were round, contained diffuse F-actin in the cytoplasm, and peripheral rings were weak or diffuse. Osteoclasts expressing Y527F c-Src, however, formed a typical peripheral F-actin ring. Resorption pit area was increased fivefold in *Lrrk1* KO osteoclasts transduced with MLV-Y527F Src compared to cells infected with MLV-GFP, with about 62% of the transduced osteoclasts showing restored bone resorptive function (data were normalized with 80% transduction efficiency). Osteoclasts expressing WT c-Src also formed a typical peripheral F-actin ring. Resorption pit area was increased 2.6-fold in *Lrrk1* KO osteoclasts transduced with MLV-WT Src compared to cells infected with MLV-GFP.

Mice with disruption of *Lrrk2* have no obvious skeletal phenotypes

Because *Lrrk2,* a paralog of *Lrrk1,* contains most domains of the ROCO family proteins and is expressed in multiple tissues and cells including monocytes,[16,17] we examined bones in 6-week-old *Lrrk2* KO mice by μCT. There were no differences in trabecular bone volume to total volume, trabecular number, or trabecular thickness in the distal femur metaphysis of *Lrrk2* KO mice compared to bones of littermate controls. Precursors derived from *Lrrk2* KO mice differentiated normally into mature TRAP-positive multinucleated osteoclasts, formed typical peripheral F-actin rings on bone slices, and differentiated osteoclasts resorbed bone. There was no significant difference in resorptive pit area between the precursors derived from *Lrrk2* KO mice and the cells from WT control littermates (Supplemental Fig. 3).

Discussion

We show that mice with disruption of the *Lrrk1* gene are severely osteopetrotic resulting from dysfunction of mature multinucleated osteoclasts with reduced bone resorption in the endocortical and trabecular regions. Total body vBMD in *Lrrk1* KO mice was the highest among 3629 distinct KO mouse lines examined in a high-throughput phenotypic screen. Long and vertebral bones from the KO mice contained extensive cancellous trabeculae with

numerous osteoclasts and retention of mineralized cartilage below growth plates. Trabecular number, trabecular thickness, and cortical thickness of the long and vertebral bones in *Lrrk1* KO mice were significantly increased. Most interestingly, *Lrrk1* KO mice had lifelong bone accumulation and responded normally to the anabolic actions of teriparatide treatment, but were resistant to OVX-induced bone boss. Our finding of osteopetrosis in *Lrrk1* KO mice provides convincing evidence that *Lrrk1* plays a critical role in regulating of bone mass in mice.

Although osteoclast precursors derived from *Lrrk1* KO mice differentiate into multinucleated cells, these osteoclasts failed to form a peripheral sealing zone, ruffled border on bone slices and to resorb bone in vitro. The phosphorylation of c-Src at Tyr-527 was significantly elevated, whereas phosphorylation of c-Src at Tyr-416 is decreased in response to M-CSF and RANKL treatment in *Lrrk1*-deficient osteoclasts. These phenotypic changes in *Lrrk1* KO osteoclasts resemble the phenotypes observed in c-Src KO osteoclasts.[38] Overexpression of a constitutively active form of the Y527F c-Src partially rescued the bone resorptive functions of Lrrk1-deficient osteoclasts, thus suggesting that Lrrk1 may function at least in part through modulating the c-Src signaling pathway. Consistent with the critical role of c-Src in bone remodeling, mice with a disruption of c-Src exhibit osteopetrosis caused by a defect in ruffled border formation and osteoclast resorptive dysfunction.[38,39]

Csk and Csk homologous kinase (Chk) inactivate c-Src by phosphorylating Tyr-527 and switching c-Src from the active open formation to an inactive closed architecture.[42,43] There is evidence that Csk is recruited to the membrane where c-Src is in an active state through Csk binding protein (Cbp).[44,45] Disruption of the Csk gene results in embryonic lethality from developmental arrest.[46] Overexpression of Csk in osteoclasts caused disorganization of the cytoskeleton, and strongly suppressed resorptive pit-formation, whereas overexpression of a kinase inactive, dominant negative Csk gene in osteoclasts increased c-Src activity and bone resorbing activity.[47] Thus, Csk is a possible target of Lrrk1. Although potential serine, threonine, and tyrosine phosphorylation sites in mouse Csk have been reported in other cell types,[42,48-50] the status of serine/threonine phosphorylation in osteoclasts is unknown. Here, we demonstrate that Lrrk1 physically interacts with Csk in RAW264.7 osteoclast precursor cells. Loss of Lrrk1 did not influence Csk expression, nor increase phosphorylation of Csk at serine 364 (data not shown). In addition, overexpression of WT Src in *Lrrk1*-null osteoclasts was not able to completely rescue the bone resorptive activity. Based on these data, together with our in vivo data showing a dramatic increase of BMD and bone volume in *Lrrk1* KO mice, and in vitro data showing increased inactivation of c-Src in *Lrrk1*-deficient cells and resorptive dysfunction of mature osteoclasts derived from *Lrrk1* KO mice on bone slices, Lrrk1 likely phosphorylates Csk at unknown serine/threonine residues and suppresses Csk kinase activity in osteoclasts. In addition, interaction of Lrrk1 with Csk may change Csk conformation or membrane translocation, leading to Csk inactivation.[41] It is possible that the active Csk in *Lrrk1* KO cells could inactivate some of the WT c-Src, which could explain why overexpression of WT c-Src did not completely rescue resorptive function in *Lrrk1* KO cells. Further studies are needed to measure endogenous Csk kinase activity and identify key serine/threonine phosphorylated residues in Csk that are modified by Lrrk1 in response to RANKL treatment or integrin activation.

Lrrk1 contains a serine/threonine kinase domain that shares sequence similarities with mitogen-activated protein kinases regulated by GTP binding to Roc domains.[12-14] There are at least three *Lrrk1* candidate tyrosine sites for additional regulation by phosphorylation.[19,20] Phosphorylation of tyrosine residues of Lrrk1 might regulate kinase/substrate interactions or kinase activity.[19] Because our studies have demonstrated Csk interacts with Lrrk1, it is possible RANK signaling phosphorylates and activates Lrrk1, and then activated Lrrk1 phosphorylates and inactivates Csk in bone cells.

We detected Lrrk2 mRNA expression in mouse bones and in osteoclast precursors. However, mice with *Lrrk2* disruption did not exhibit any obvious skeletal phenotypes. Osteoclast precursors derived from *Lrrk2* KO mice differentiated into TRAP-positive multinucleated cells in response to M-CSF and RANKL treatment, and the cells formed a peripheral sealing zone, ruffled border, and degraded bone similarly to WT osteoclasts. Our data suggest that *Lrrk1* and *Lrrk2* have distinct functions in certain tissues (e.g., *Lrrk1* in bone and *Lrrk2* in the nervous system) and that *Lrrk2* cannot compensate for the loss of *Lrrk1* or vice versa to fulfill specific functions.

Although both Lrrk1 and Lrrk2 contain common functional domains, Lrrk1 contains N-terminal ankyrin repeats, whereas Lrrk2 has specific repeats with unknown functions.[15] Because ankyrin repeats are known protein-protein interaction motifs, Lrrk1 signal pathways are likely distinct from those of Lrrk2. The unique structure of ankyrin repeats at the N-terminus of Lrrk1 might be involved in the interaction with specific kinase substrates, and/or formation of a scaffold to regulate signal molecules in response to a variety of bone resorption regulators. The ankyrin repeat of osteoclast-stimulating factor (OSF) interacts with c-Src or other Src-related proteins through its SH3/ankyrin-repeat domains to promote osteoclast formation and bone resorption.[51,52] In addition, an ankyrin-repeat, SH3-domain- and proline-rich-region containing protein (dASPP) binds with Drosophila Csk and modulates its activity.[53] The lack of a skeletal phenotype in *Lrrk2* KO mice is consistent with Lrrk1 ankyrin repeats mediating specific substrate interactions.[15] Lrrk1 and Lrrk2 might phosphorylate different substrates as the amino acid sequences of their kinase domains are not highly conserved. Our future work will examine roles of the Lrrk1 ankyrin repeats in regulating key functional protein/protein interactions, identify the critical resides of ankyrin repeats required for binding to Csk by site-directed mutagenesis and protein binding assays, and search for other peptide ligands or small molecules by crystal structure–based drug design and docking.

Because mice lacking Lrrk1 exhibited a more severe osteopetrotic phenotype than c-Src KO mice, Lrrk1 may interact with upstream pathways in addition to the c-Src signaling pathway. A recent study has shown that c-Src binds to activated RANKL via its SH2 domain and αvβ3 via its SH3 domain, suggesting c-Src links these two receptors.[54] In preliminary studies, we observed that Lrrk1 physically associates with RANK (data not shown). It remains to be determined if the Lrrk1 ankyrin repeats are involved in facilitating formation of complexes involving RANK, integrin avb3, Lrrk1,Csk, and c-src. Alternatively, Lrrk1 may crosstalk with signaling proteins whose functions are yet to be clarified. Future studies identifying other Lrrk1 interacting partners in osteoclasts will help in understanding the key mechanisms that contribute to the severe osteopetrosis in *Lrrk1* KO mice.

Supplementary Material

Refer to Web version on PubMed Central for supplementary material.

Acknowledgments

This work was supported by National Institutes of Health grants R21AR056833 (to WX) and R01AR31062 (to SM). The funder had no role in study design, data collection and analysis, decision to publish, or manuscript preparation. The authors thank Catrina Alarcon, Heather Watt, Joe Rung-Aroon, and Sheila Pourteymoor for their technical assistance (Loma Linda). We also thank Deon Smith for P1NP and TRAP5b assays, Rose Champ for embedding bones in plastic, Wendy Xiong for μCT scans and bone sectioning, Andrea Y. Thompson for microscopy, Sabrina Jeter-Jones for dosing teriparatide, Laura Kirkpatrick for reviewing the KO strategy, the Pathology group for embedding and staining bones in paraffin, and Larry Rodriquez for vBMD database analysis (Lexicon). We thank Thomas J. Wronski of the University of Florida for providing von Kossa–stained plastic sections showing osteopetrosis during the initial characterization of *Lrrk1* KO mice. Imaging was performed in the LLUSM Advanced Imaging and Microscopy Core funded by the NSF (MRI-DBI 092355) and LLUSM. The Department of Veterans Affairs in Loma Linda, CA, USA, provided facilities to carry out the majority of this work.

References

1. Segovia-Silvestre T, Neutzsky-Wulff AV, Sorensen MG, Christiansen C, Bollerslev J, Karsdal MA, Henriksen K. Advances in osteoclast biology resulting from the study of osteopetrotic mutations. Hum Genet. 2009;124(6):561–77. [PubMed: 18987890]
2. Feng X, McDonald JM. Disorders of bone remodeling. Annu Rev Pathol. 2011;6:121–45. [PubMed: 20936937]
3. Redlich K, Smolen JS. Inflammatory bone loss: pathogenesis and therapeutic intervention. Nat Rev Drug Discov. 2012;11(3): 234–50. [PubMed: 22378270]
4. Glaser DL, Kaplan FS. Osteoporosis. Definition and clinical presentation. Spine (Phila Pa 1976). 1997 Dec 15;22(24 Suppl):12S–16S. [PubMed: 9431639]
5. Deal C Bone loss in rheumatoid arthritis: systemic, periarticular, and focal. Curr Rheumatol Rep. 2012;14(3):231–7. [PubMed: 22527950]
6. Pepelassi E, Nicopoulou-Karayianni K, Archontopoulou A, Mitsea A, Kavadella A, Tsiklakis K, Vrotsos I, Devlin H, Horner K. The relationship between osteoporosis and periodontitis in women aged 45–70. years. Oral Dis. 2012;18(4):353–9. [PubMed: 22151499]
7. Suleiman Martos Y, Avilés Pérez MD, Escobar Jimenez F, Muñoz Torres ME. [Multiple myeloma as a cause of rapidly progressive osteoporosis]. Endocrinol Nutr. 2012 Jun-Jul;59(6):398–400. Spanish. [PubMed: 22281293]
8. [No authors listed.] Denosumab. Limited efficacy in fracture prevention, too many adverse effects. Prescrire Int. 2011;20(117): 145–8. [PubMed: 21678700]
9. Kidd LJ, Cowling NR, Wu AC, Kelly WL, Forwood MR. Bisphosphonate treatment delays stress fracture remodeling in the rat ulna. J Orthop Res. 2011;29(12):1827–33. [PubMed: 21598308]
10. Nase JB, Suzuki JB. Osteonecrosis of the jaw and oral bisphosphonate treatment. J Am Dent Assoc. 2006;137(8):1115–9; quiz 1169–70. [PubMed: 16873327]
11. Taylor KH, Middlefell LS, Mizen KD. Osteonecrosis of the jaws induced by anti-RANK ligand therapy. Br J Oral Maxillofac Surg. 2010;48(3): 221–3. [PubMed: 19836866]
12. Bosgraaf L, Van Haastert PJ. Roc, a Ras/GTPase domain in complex proteins. Biochim Biophys Acta. 2003;1643(1–3):5–10. [PubMed: 14654223]
13. Mosavi LK, Cammett TJ, Desrosiers DC, Peng ZY. The ankyrin repeat as molecular architecture for protein recognition. Protein Sci. 2004; 13(6):1435–48. [PubMed: 15152081]
14. Kobe B, Kajava AV. The leucine-rich repeat as a protein recognition motif. Curr Opin Struct Biol. 2001;11(6):725–32. [PubMed: 11751054]
15. Marin I. The Parkinson disease gene LRRK2: evolutionary and structural insights. Mol Biol Evol. 2006;23(12):2423–33. [PubMed: 16966681]

16. Biskup S, Moore DJ, Rea A, Lorenz-Deperieux B, Coombes CE, Dawson VL, Dawson TM, West AB. Dynamic and redundant regulation of LRRK2 and LRRK1 expression. BMC Neurosci. 2007;8:102. [PubMed: 18045479]

17. Takahashi Y, Miyata M, Zheng P, Imazato T, Horwitz A, Smith JD. Identification of cAMP analogue inducible genes in RAW264 macrophages. Biochim Biophys Acta. 2000;1492(2–3):385–394. [PubMed: 11004510]

18. Korr D,Toschi L, Donner P, Pohlenz HD, Kreft B, Weiss B. LRRK1 protein kinase activity is stimulated upon binding of GTP to its Roc domain. Cell Signal. 2006;18(6):910–20. [PubMed: 16243488]

19. Titz B, Low T, Komisopoulou E, Chen SS, Rubbi L, Graeber TG. The proximal signaling network of the BCR-ABL1 oncogene shows a modular organization. Oncogene. 2010;29(44):5895–10. [PubMed: 20697350]

20. Ishikawa K, Nara A, Matsumoto K, Hanafusa H. EGFR-dependent phosphorylation of leucine-rich repeat kinase LRRK1 is important for proper endosomal trafficking of EGFR. Mol Biol Cell. 2012;23 (7):1294–306. [PubMed: 22337768]

21. Zimprich A, Biskup S, Leitner P, Lichtner P, Farrer M, Lincoln S, Kachergus J, Hulihan M, Uitti RJ, Calne DB, Stoessl AJ, Pfeiffer RF, Patenge N, Carbajal IC, Vieregge P, Asmus F, Muller-Myhsok B, Dickson DW, Meitinger T, Strom TM, Wszolek ZK, Gasser T. Mutations in LRRK2 cause autosomal-dominant parkinsonism with pleomorphic pathology. Neuron. 2004;44(4):601–7. [PubMed: 15541309]

22. Smith WW, Pei Z, Jiang H, Dawson VL, Dawson TM, Ross CA. Kinase activity of mutant LRRK2 mediates neuronal toxicity. Nat Neurosci. 2006;9(10):1231–3. [PubMed: 16980962]

23. Herzig MC, Kolly C, Persohn E, Theil D, Schweizer T, Hafner T, Stemmelen C, Troxler TJ, Schmid P, Danner S, Schnell CR, Mueller M, Kinzel B, Grevot A, Bolognani F, Stirn M, Kuhn RR, Kaupmann K, van der Putten PH, Rovelli G, Shimshek DR. LRRK2 protein levels are determined by kinase function and are crucial for kidney and lung homeostasis in mice. Hum Mol Genet. 2011;20(21):4209–23. [PubMed: 21828077]

24. Zambrowicz BP, Abuin A, Ramirez-Solis R, Richter LJ, Piggott J, BeltrandelRio H, Buxton EC, Edwards J, Finch RA, Friddle CJ, Gupta A, Hansen G, Hu Y, Huang W, Jaing C, Key BW Jr, Kipp P, Kohlhauff B, Ma ZQ, Markesich D, Payne R, Potter DG, Qian N, Shaw J, Schrick J, Shi ZZ, Sparks MJ, Van Sligtenhorst I, Vogel P, Walke W, Xu N, Zhu Q, Person C, Sands AT. Wnk1 kinase deficiency lowers blood pressure in mice: a gene-trap screen to identify potential targets for therapeutic intervention. Proc Natl Acad Sci U S A. 2003;100(24):14109–14. [PubMed: 14610273]

25. Donoviel DB, Freed DD, Vogel H, Potter DG, Hawkins E, Barrish JP, Mathur BN, Turner CA, Geske R, Montgomery CA, Starbuck M, Brandt M, Gupta A, Ramirez-Solis R, Zambrowicz BP, Powell DR. Proteinuria and perinatal lethality in mice lacking NEPH1, a novel protein with homology to NEPHRIN. Mol Cell Biol. 2001;21(14):4829–36. [PubMed: 11416156]

26. Brommage R, Desai U, Revelli JP, Donoviel DB, Fontenot GK, Dacosta CM, Smith DD, Kirkpatrick LL, Coker KJ, Donoviel MS, Eberhart DE, Holt KH, Kelly MR, Paradee WJ, Philips AV, Platt KA, Suwanichkul A, Hansen GM, Sands AT, Zambrowicz BP, Powell DR. High-throughput screening of mouse knockout lines identifies true lean and obese phenotypes. Obesity (Silver Spring). 2008;16(10):2362–7. [PubMed: 18719666]

27. Bouxsein ML, Boyd SK, Christiansen BA, Guldberg RE, Jepsen KJ, Muller R. Guidelines for assessment of bone microstructure in rodents using micro-computed tomography. J Bone Miner Res. 2010;25(7): 1468–86. [PubMed: 20533309]

28. Xing W, Pourteymoor S, Mohan S. Ascorbic acid regulates osterix expression in osteoblasts by activation of prolyl hydroxylase and ubiquitination-mediated proteosomal degradation pathway. Physiol Genomics. 2011;43(12):749–57. [PubMed: 21467157]

29. Xing W, Kim J, Wergedal J, Chen ST, Mohan S. Ephrin B1 regulates bone marrow stromal cell differentiation and bone formation by influencing TAZ transactivation via complex formation with NHERF1. Mol Cell Biol. 2010;30(3):711–21. [PubMed: 19995908]

30. Zheng HF, Tobias JH, Duncan E, Evans DM, Eriksson J, Paternoster L, Yerges-Armstrong LM, Lehtimaki T, Bergstrom U, Kahonen M, Leo PJ, Raitakari O, Laaksonen M, Nicholson GC, Viikari J, Ladouceur M, Lyytikainen LP, Medina-Gomez C, Rivadeneira F, Prince RL, Sievanen

H, Leslie WD, Mellstrom D, Eisman JA, Moverare-Skrtic S, Goltzman D, Hanley DA, Jones G, St Pourcain B, Xiao Y,Timpson NJ, Smith GD, Reid IR, Ring SM, Sambrook PN, Karlsson M, Dennison EM, Kemp JP, Danoy P, Sayers A, Wilson SG, Nethander M, McCloskey E, Vandenput L, Eastell R, Liu J, Spector T, Mitchell BD, Streeten EA, Brommage R, Pettersson-Kymmer U, Brown MA, Ohlsson C, Richards JB, Lorentzon M. WNT16 influences bone mineral density, cortical bone thickness, bone strength, and osteoporotic fracture risk. PLoS Genet. 2012;8(7): e1002745. [PubMed: 22792071]

31. Beamer WG, Donahue LR, Rosen CJ, Baylink DJ. Genetic variability in adult bone density among inbred strains of mice. Bone. 1996;18(5): 397–403. [PubMed: 8739896]
32. Qin X, Wergedal JE, Rehage M, Tran K, Newton J, Lam P, Baylink DJ, Mohan S. Pregnancy-associated plasma protein-A increases osteoblast proliferation in vitro and bone formation in vivo. Endocrinology 2006;147(12):5653–61. [PubMed: 16946002]
33. Parfitt AM, Drezner MK, Glorieux FH, Kanis JA, Malluche H, Meunier PJ, Ott SM, Recker RR. Bone histomorphometry: standardization of nomenclature, symbols, and units. Report of the ASBMR Histomorphometry Nomenclature Committee. J Bone Miner Res. 1987; 2(6):595–610. [PubMed: 3455637]
34. Leeming DJ, Larsen DV, Zhang C, Hi Y, Veidal SS, Nielsen RH, Henriksen K, Zheng Q, Barkholt V, Riis BJ, Byrjalsen I, Qvist P, Karsdal MA. Enzyme-linked immunosorbent serum assays (ELISAs) for rat and human N-terminal pro-peptide of collagen type I (PINP)—assessment of corresponding epitopes. Clin Biochem. 2010;43(15):1249–56. [PubMed: 20709044]
35. Xing W, Baylink D, Kesavan C, Mohan S. HSV-1 amplicon-mediated transfer of 128-kb BMP-2 genomic locus stimulates osteoblast differentiation in vitro. Biochem Biophys Res Commun. 2004;319(3): 781–6. [PubMed: 15184051]
36. Cheng S, Zhao SL, Nelson B, Kesavan C, Qin X, Wergedal J, Mohan S, Xing W. Targeted disruption of ephrin b1 in cells of myeloid lineage increases osteoclast differentiation and bone resorption in mice. PLoS One. 2012;7(3):e32887. [PubMed: 22403721]
37. Xing W, Singgih A, Kapoor A, Alarcon CM, Baylink DJ, Mohan S. Nuclear factor-E2-related factor-1 mediates ascorbic acid induction of osterix expression via interaction with antioxidant-responsive element in bone cells. J Biol Chem. 2007;282(30):22052–61. [PubMed: 17510056]
38. Lowe C, Yoneda T, Boyce BF, Chen H, Mundy GR, Soriano P. Osteopetrosis in Src-deficient mice is due to an autonomous defect of osteoclasts. Proc Natl Acad Sci U S A. 1993;90(10):4485–9. [PubMed: 7685105]
39. Nakayama H, Takakuda K, Matsumoto HN, Miyata A, Baba O, Tabata MJ, Ushiki T, Oda T, McKee MD, Takano Y. Effects of altered bone remodeling and retention of cement lines on bone quality in osteopetrotic aged c-Src-deficient mice. Calcif Tissue Int. 2010; 86(2):172–83. [PubMed: 20063091]
40. Miyazaki T, Tanaka S, Sanjay A, Baron R. The role of c-Src kinase in the regulation of osteoclast function. Mod Rheumatol. 2006;16(2):68–74. [PubMed: 16633924]
41. Okada M. Regulation of the SRC family kinases by Csk. Int J Biol Sci. 2012;8(10):1385–97. [PubMed: 23139636]
42. Joukov V, Vihinen M, Vainikka S, Sowadski JM, Alitalo K, Bergman M. Identification of csk tyrosine phosphorylation sites and a tyrosine residue important for kinase domain structure. Biochem J. 1997;322 (Pt 3): 927–35. [PubMed: 9148770]
43. Lee S, Lin X, Nam NH, Parang K, Sun G. Determination of the substrate-docking site of protein tyrosine kinase C-terminal Src kinase. Proc Natl Acad Sci U S A 2003;100(25):14707–12. [PubMed: 14657361]
44. Kawabuchi M, Satomi Y, Takao T, Shimonishi Y, Nada S, Nagai K, Tarakhovsky A, Okada M. Transmembrane phosphoprotein Cbp regulates the activities of Src-family tyrosine kinases. Nature 2000;404 (6781):999–1003. [PubMed: 10801129]
45. Matsuoka H, Nada S, Okada M. Mechanism of Csk-mediated down-regulation of Src family tyrosine kinases in epidermal growth factor signaling. J Biol Chem. 2004;279(7):5975–83. [PubMed: 14613929]

46. Imamoto A, Soriano P. Disruption of the csk gene, encoding a negative regulator of Src family tyrosine kinases, leads to neural tube defects and embryonic lethality in mice. Cell. 1993;73(6): 1117–24. [PubMed: 7685657]

47. Miyazaki T, Takayanagi H, Isshiki M, Takahashi T, Okada M, Fukui Y, Oda H, Nakamura K, Hirai H, Kurokawa T, Tanaka S. In vitro and in vivo suppression of osteoclast function by adenovirus vector-induced csk gene. J Bone Miner Res. 2000;15(1):41–51. [PubMed: 10646113]

48. Sun G, Ke S, Budde RJ. Csk phosphorylation and inactivation in vitro by the cAMP-dependent protein kinase. Arch Biochem Biophys. 1997;343(2):194–200. [PubMed: 9224730]

49. Vang T, Torgersen KM, Sundvold V, Saxena M, Levy FO, Skalhegg BS, Hansson V, Mustelin T,Tasken K. Activation of the COOH-terminal Src kinase (Csk) by cAMP-dependent protein kinase inhibits signaling through the T cell receptor. J Exp Med. 2001;193(4):497–507. [PubMed: 11181701]

50. Baker MA, Hetherington L, Aitken RJ. Identification of SRC as a key PKA-stimulated tyrosine kinase involved in the capacitation-associated hyperactivation of murine spermatozoa. J Cell Sci. 2006; 119 (Pt 15): 3182–92. [PubMed: 16835269]

51. Chen L, Wang Y, Wells D, Toh D, Harold H, Zhou J, DiGiammarino E, Meehan EJ. Structure of the SH3 domain of human osteoclast-stimulating factor at atomic resolution. Acta Crystallogr Sect F Struct Biol Cryst Commun. 2006;62 (Pt 9): 844–8.

52. Reddy S, Devlin R, Menaa C, Nishimura R, Choi SJ, Dallas M, Yoneda T, Roodman GD. Isolation and characterization of a cDNA clone encoding a novel peptide (OSF) that enhances osteoclast formation and bone resorption. J Cell Physiol. 1998;177(4):636–45. [PubMed: 10092216]

53. Langton PF, Colombani J, Aerne BL, Tapon N. Drosophila ASPP regulates C-terminal Src kinase activity. Dev Cell. 2007;13(6): 773–82. [PubMed: 18061561]

54. Izawa T, Zou W, Chappel JC, Ashley JW, Feng X, Teitelbaum SL. c-Src links a RANK/alphavbeta3 integrin complex to the osteoclast cytoskeleton. Mol Cell Biol. 2012;32(14):2943–53. [PubMed: 22615494]

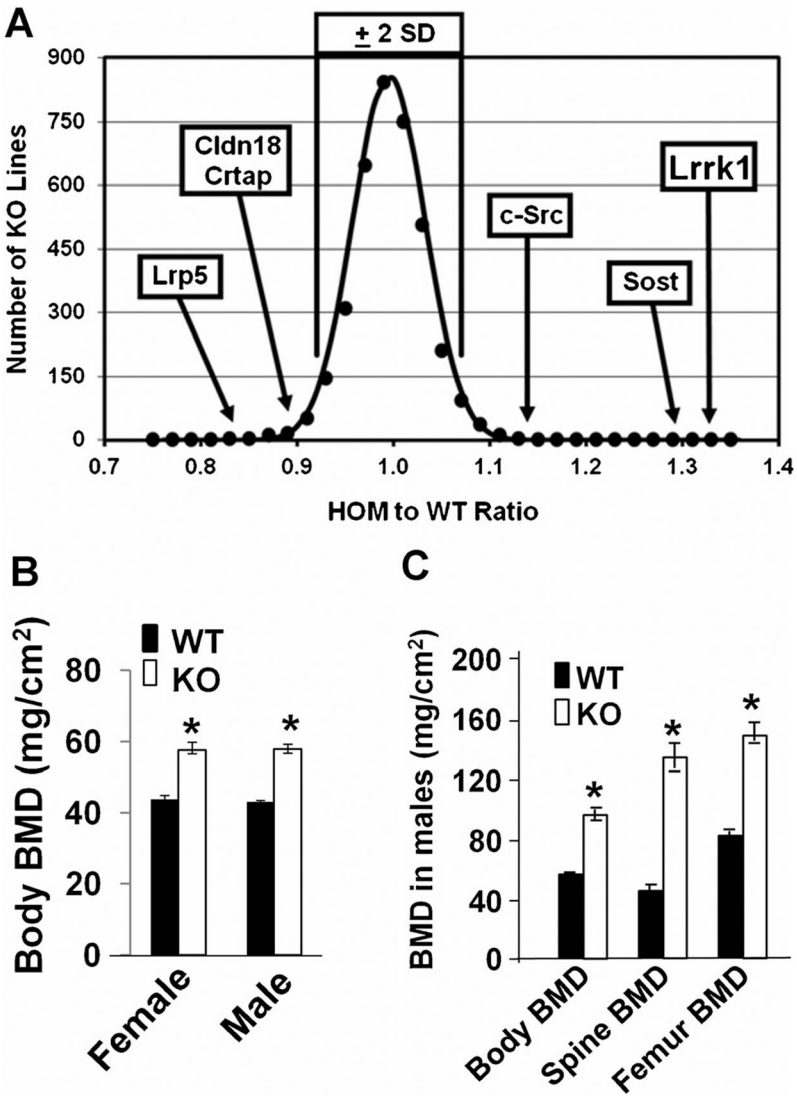

Fig. 1.

Lrrk1$^{-/-}$ mice have increased bone mineral density (BMD). (*A*) KO of *Lrrk1* results in the highest observed vBMD among 3629 KO mouse lines. A histogram of the 14-week-old homozygous to WT mouse vBMD ratio is plotted with vBMD ratio data from 3629 distinct KO mouse lines compared to WT littermate mice, measured by DXA. (*B*) Total body BMD is increased in 6-week-old *Lrrk1* KO mice. Values are expressed as mean ± SEM. A star represents statistical significance in *Lrrk1*$^{-/-}$ mice compared to the corresponding littermate controls ($p < 0.01$, $n = 8$). (*C*) Total body BMD, vertebra BMD, and femur BMD are increased in 70-week-old male mice. Values are expressed as mean ± SEM. A star represents statistical significance in *Lrrk1* KO mice compared to the corresponding littermate controls ($p < 0.01$, $n = 9$).

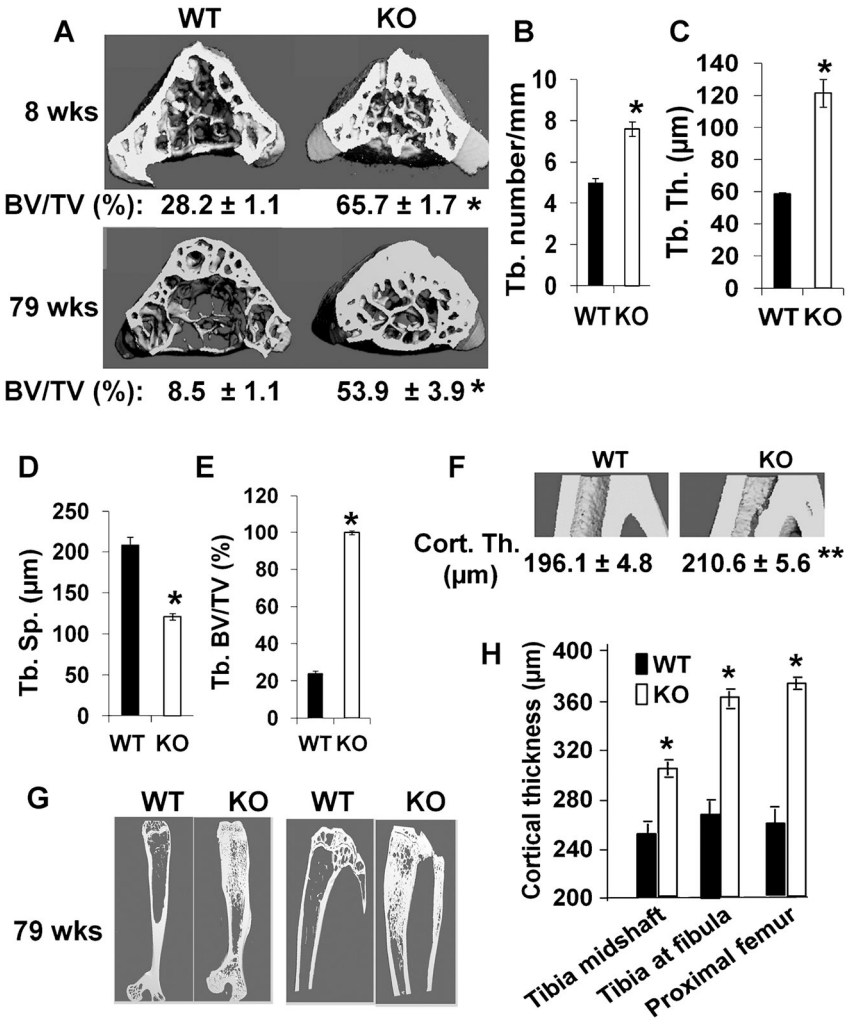

Fig. 2.

Lrrk1$^{-/-}$ mice exhibit osteopetrosis as shown by μCT scans. (*A*) Cross-section of lumbar vertebra 5 (L_5) of 8-week-old and 79-week old WT and KO males. Quantitative data of 8-week-old mice ($n = 8$, with 4 males and 4 females) and 79-week-old males ($n = 7–9$) are presented below the images. (*B–D*) Quantitative measurements of trabecular number (Tb.N), trabecular thickness (Tb.Th), and trabecular spacing (Tb.Sp) at the middle of L_5 of 8-week old mice. (*E*) Quantitative measurements of trabecular bone at the metaphysis of proximal tibia of 8-week-old WT and KO mice. (*F*) Longitudinal sections of μCT images of tibia from 8-week-old WT and KO mice at the fibular junction. Quantitative measurements of cortical thickness are presented below the panel. (*G*) Longitudinal sections of μCT images of the femur and tibia of 79-week-old WT and KO males. (*H*) Quantitative measurements of cortical thickness at the tibia of 79-week-old WT and KO males. Values are expressed as mean ± SEM ($n = 8–9$). A star represents statistical significance ($p < 0.01$) when compared to WT littermate controls.

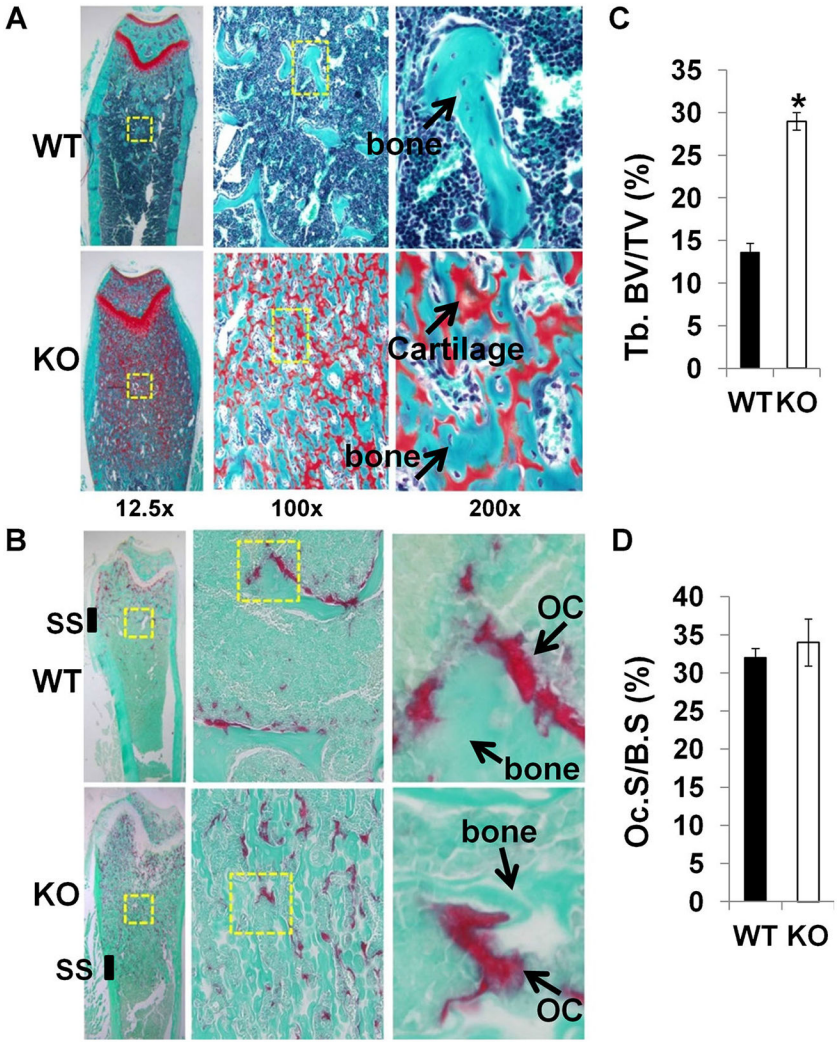

Fig. 3.

Disruption of *Lrrk1* impairs osteoclast activity and decreases bone resorption. (*A*) Distal femurs from 12-week-old *Lrrk1* KO females contain extensive cancellous trabeculae and expansion of mineralized cartilage below the growth plate. Longitudinal bone sections are stained with Safranin O and methyl green. Arrows indicate orange stained cartilage, and green stained trabecular bone. (*B*) Distal femurs from 8-week-old *Lrrk1* KO females contain numerous mature osteoclasts (OCs). Arrows show representative TRAP-positive osteoclasts present on surfaces of metaphyseal trabeculae. (*C*) Histomorphometric measurement of trabecular bone volume/total volume (%) at the secondary spongiosa (SS) of the distal femur metaphysic of 12-week-old mice ($n = 8$, with 4 females and 4 males in two batches). (*D*) Quantitative data of the TRAP-labeled surface to bone surface (Tb.S/BS) measured at the secondary spongiosa of the distal metaphysis of the femur of 12-week-old mice. Values are presented as mean ± SEM. A star presents statistical significance ($p < 0.01$) when compared to WT littermate controls.

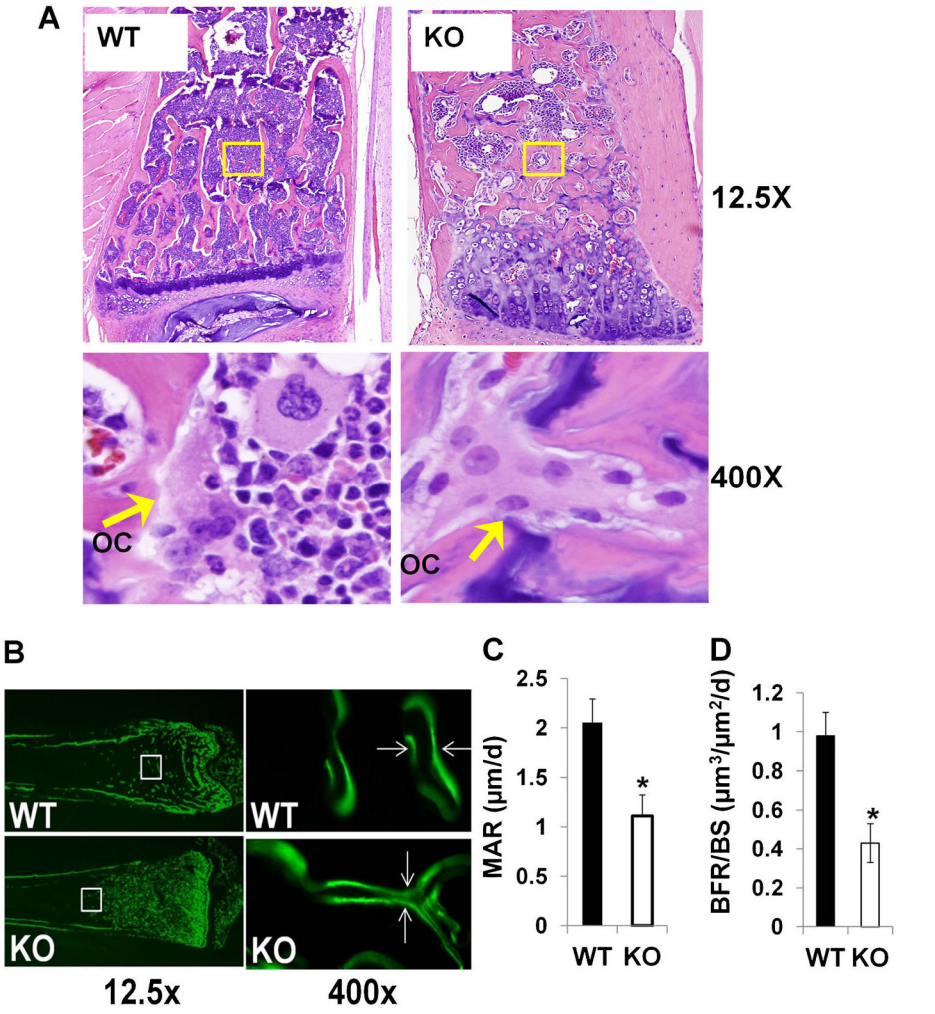

Fig. 4.

Reduced bone resorption and bone formation rate in *Lrrk1* KO mice. (*A*) Longitudinal bone sections of L_5 of 79-week-old male mice. Bone sections are stained with hematoxylin and eosin. Arrows indicate osteoclasts (OCs) within the areas indicated. (*B*) Images of calcein double-labeling of the femurs from 8-week-old mice. Mineral apposition rate (MAR) (*C*) and bone formation rate (BFR) (*D*) within the areas indicated. Data are means ± SEM for $n = 8$. Asterisks indicate a significant difference in KO mice compared with WT mice ($p < 0.01$).

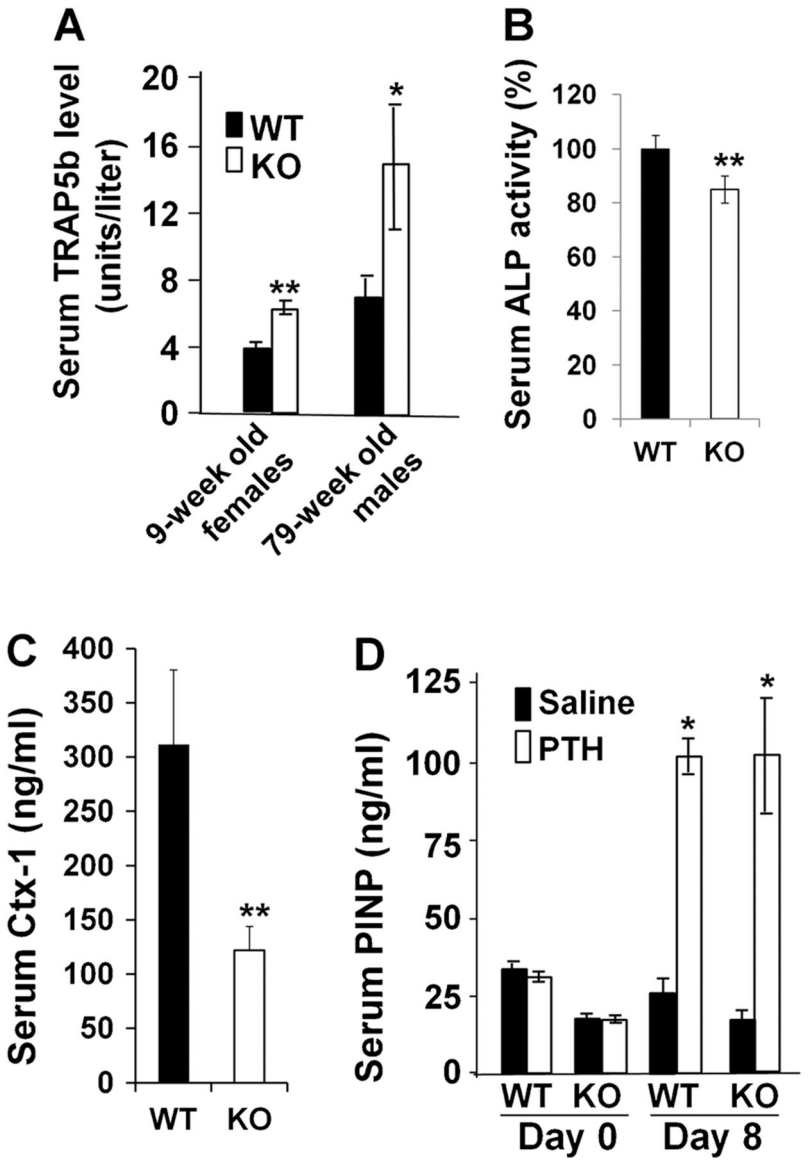

Fig. 5.

Lrrk1 KO mice have elevated levels of serum TRAP5b, reduced serum P1NP and ALP levels, but exhibit a normal anabolic response to teriparatide treatment. (*A*) Serum TRAP5b levels in female 9-week-old (n = 10 and 12) and male 79-week-old (n = 7–6) mice. (*B*) Serum ALP activity in 8-week-old mice (n = 8, with 4 males and 4 females). (*C*) Serum collagen I C-terminal propeptide (Ctx-1) levels in male 4-week-old WT and *Lrrk1* KO mice (n = 5). Data are means ± SEM. (*D*) Serum procollagen I N-terminal propeptide (P1NP) levels in male 70-week-old mice at baseline and in response to teriparatide treatment (n = 4–5). Data are means ± SEM.

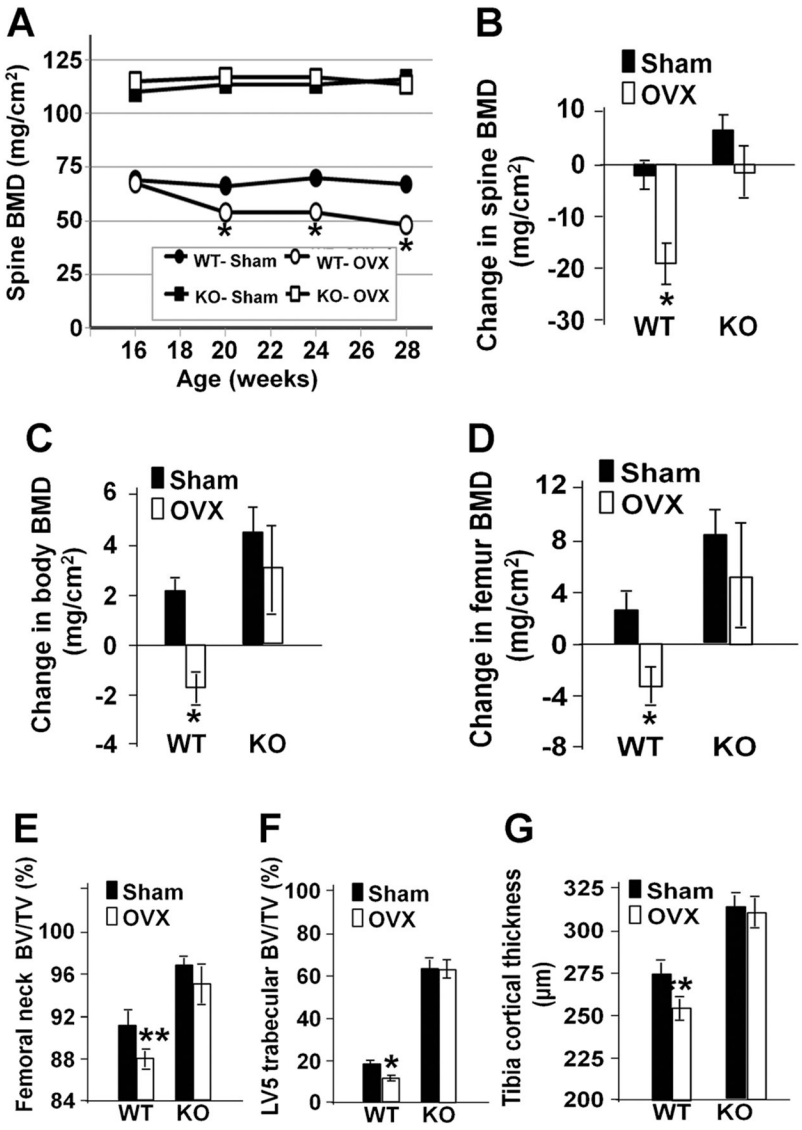

Fig. 6.

Lrrk1 KO mice are protected against OVX-induced bone loss. (*A*) Time-course of spine BMD at baseline and 4, 8, and 12 weeks after surgery at 16 weeks of age ($n = 4$). Changes in spin BMD (*B*), total body BMD (*C*), and femur BMD (*D*) 12 weeks after surgery. µCT analyses of femoral neck BV/TV (*E*), L_5 mid-region trabecular BV/TV (*F*), and tibia shaft cortical thickness (*G*) 12 weeks after surgery. Data are means ± SEM for 11 or 12 mice per group. Single and double asterisks indicate significant differences in OVX mice compared with control sham mice at $p < 0.01$ and $p < 0.05$, respectively.

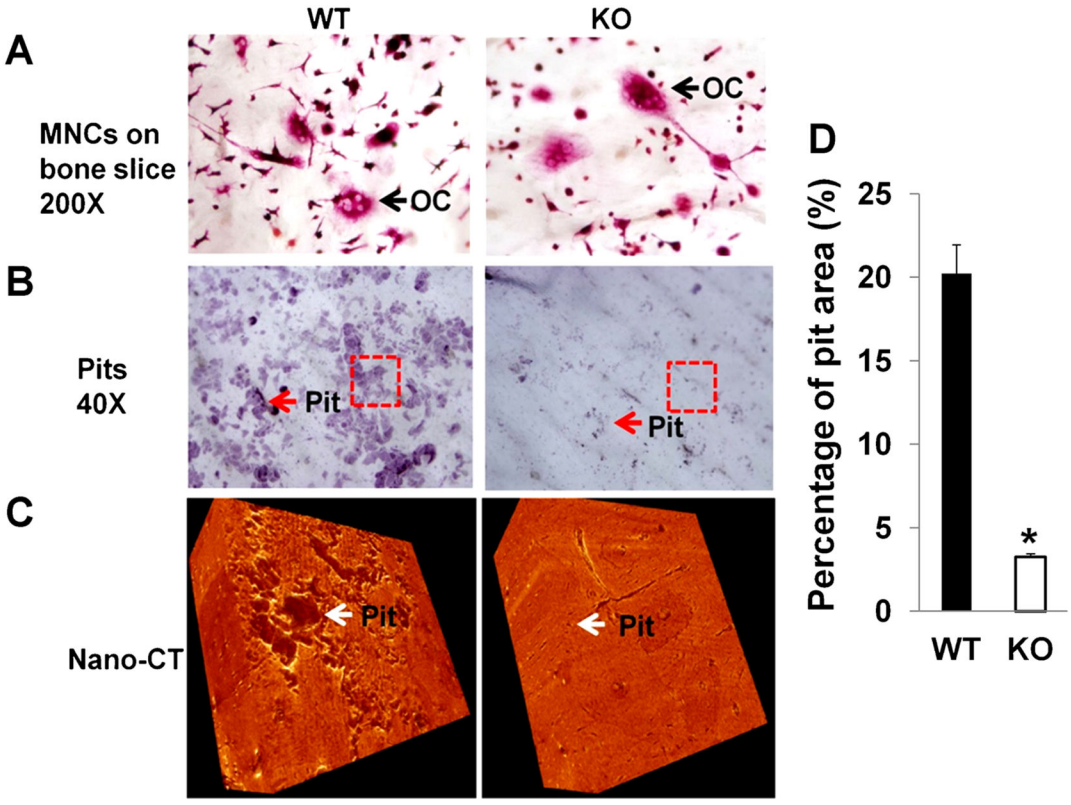

Fig. 7.

Osteoclasts lacking *Lrrk1* have a defect in bone resorptive function. (*A*) TRAP-positive osteoclasts on bone slices. Monocytes derived from spleens of *Lrrk1* KO and WT mice were differentiated on bone slices for 6 days, followed by TRAP staining. The arrow identifies osteoclast (OC). (*B*) Pit formation. Monocytes derived from spleens of *Lrrk1* KO and WT mice were differentiated on bone slices for 10 days. Cells were removed, and pits were stained with hematoxylin. Arrows point to stained pits. Rectangles are selected areas for nano-CT analyses. (*C*) 3D images of pits on bone slices scanned with nano-CT. Arrows point to pits in selected areas. (*D*) Quantitative data of pit formation from *B* ($n = 6$). Data are means ± SEM. An asterisk indicates a significant difference in osteoclasts derived from *Lrrk1* KO mice compared with the cells derived from WT control mice ($p < 0.01$).

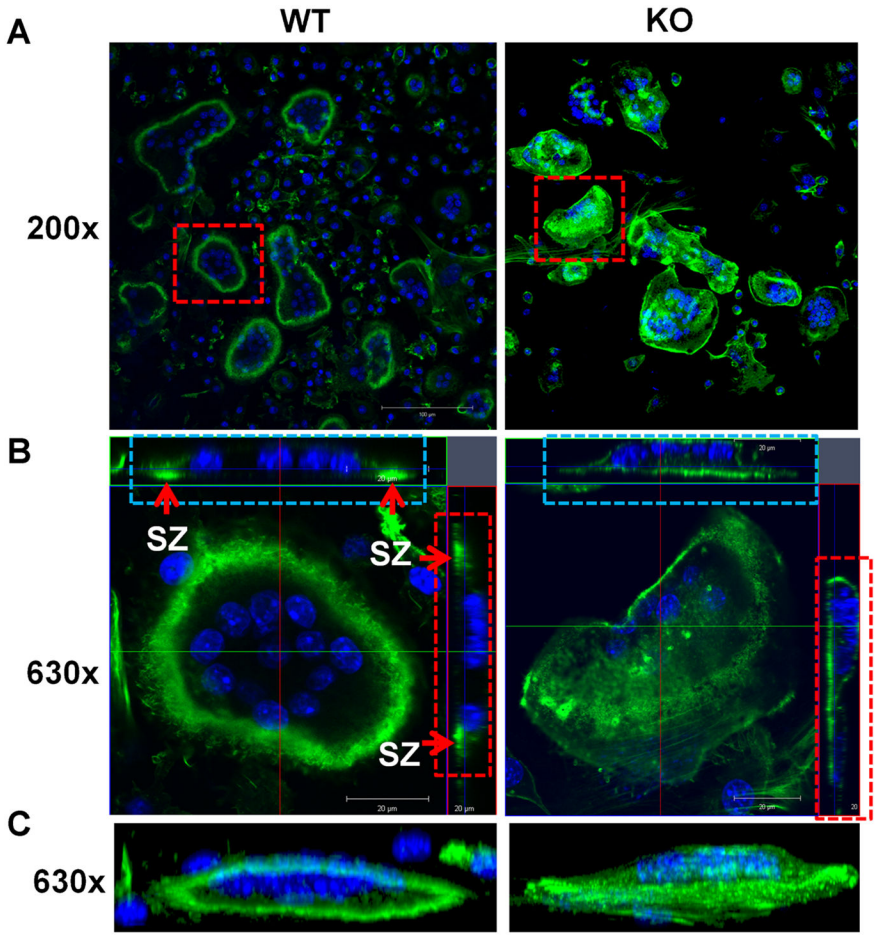

Fig. 8.

Osteoclasts lacking *Lrrk1* fail to form a peripheral sealing zone (SZ). (*A*) F-actin ring formation on bone slices in horizontal cross-section. Monocytes derived from spleens of *Lrrk1* KO and WT mice were differentiated on bone slices for 6 days, followed by F-actin immunostaining and confocal microscope analyses. Squares are selected mature osteoclasts for 3D high-magnification analyses in *B*. (*B*) Horizontal cross sections of selected osteoclasts in *A*. Two lines in green and red in the middle of the cell represent positions of horizontal and vertical cut, respectively. Rectangles in blue and red are orthogonal views of *x* and *y*-section, respectively. Arrows indicate sealing zones (two green dots in WT cell, but a green line in *Lrrk1* KO cell). (*C*) 3D rendering of a lateral view. Nuclei are stained blue with DAPI. Experiments were repeated three times, and representative images are shown.

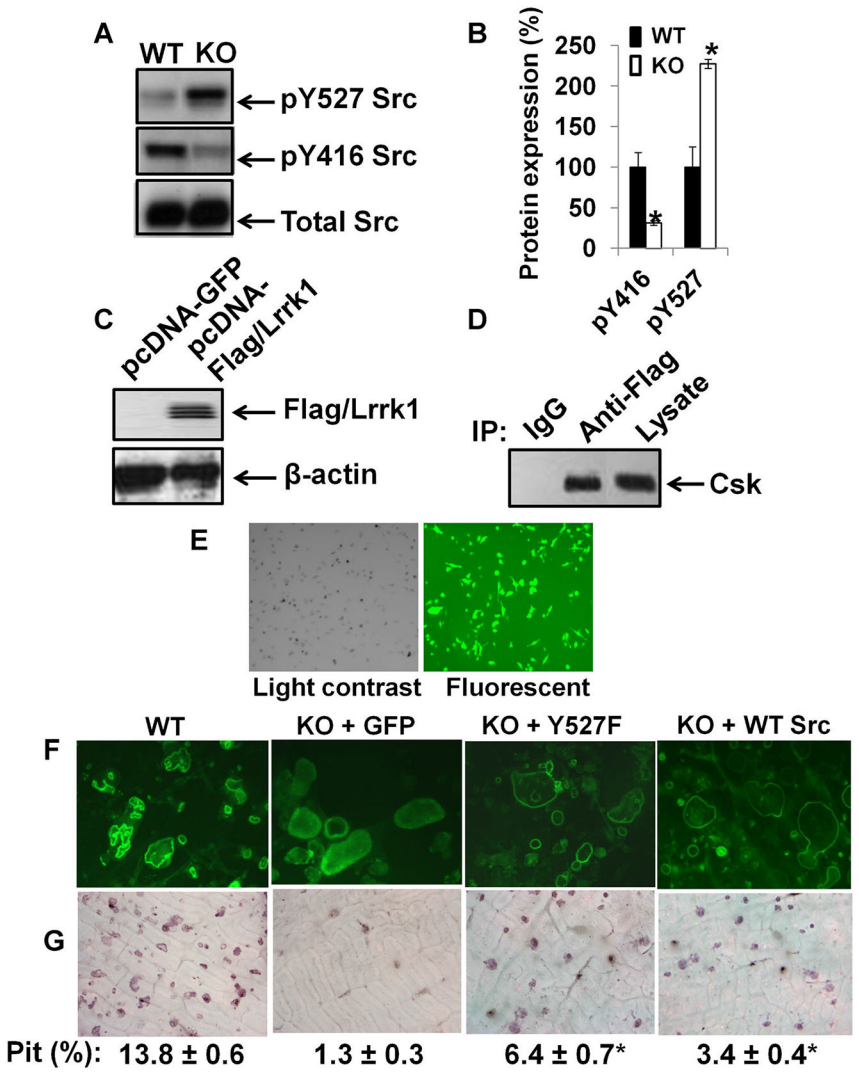

Fig. 9.

Lrrk1 interacts with Csk, and is involved in the regulation of c-Src phosphorylation. (*A*) Increased pY527 c-Src and decreased pY416 c-Src in *Lrrk1* KO osteoclasts. A representative image of a Western blot is shown. (*B*) Quantitative data from Western blots from three independent experiments with three replicates each time. (*C*) Overexpression of human Lrrk1 (hLrrk1) and Flag fusion protein in RAW264.7 cells. (*D*) Interaction of hLrrk1 with Csk in transiently transfected RAW264.7 cells, detected by immunoprecipitation. (*E*) High efficiency of MLV-mediated transduction in Lrrk1-deficient osteoclast precursors, as measured using a GFP reporter. (*F*) F-actin ring formation in osteoclasts expressing GFP and Y527F Src, respectively. (*G*) Overexpression of constitutively active c-Src in Lrrk1-deficient osteoclasts rescues bone resorptive function. Primary osteoclast precursors derived from spleens of *Lrrk1* KO mice were transduced with MLV-GFP, MLV-Y527F, or MLV-WT Src. Cells were differentiated on bone slices for pit formation assays.